Asian Journal of Chemistry; Vol. 25, No. 2 (2013), 701-707

ASIAN JOURNAL OF CHEMISTRY

http://dx.doi.org/10.14233/ajchem.2013.12566

Influence of $[B_{mim}]HSO_4$ on the Nucleation and Growth of Zinc on Aluminum from Acidic Sulphate Bath

Q.B. ZHANG* and Y.X. HUA

Key Laboratory of Ionic Liquids Metallurgy, Faculty of Metallurgical and Energy Engineering, Kunming University of Science and Technology, Kunming 650093, P.R. China

*Corresponding author: Fax: +86 871 5161278; Tel: +86 871 5162008; E-mail: qibozhang@yahoo.com.cn

(*Received*: 12 August 2011; *Accepted*: 14 August 2012) AJC-11960

The effect of ionic liquid additive 1-butyl-3-methylimidazolium hydrogen sulphate-$[B_{mim}]HSO_4$ on the nucleation and growth of zinc on aluminum from a 0.1 M $ZnSO_4$ + 0.5 M Na_2SO_4 solution were investigated using cyclic voltammetry, chrono- amperometric current-time transients and scanning electron microscopy techniques. Dimensionless chronoamperometric current-time transients for zinc electrodeposition from the solution free of $[B_{mim}]HSO_4$ were in good agreement with the theoretical transients for the limiting case of progressive nucleation with hemispherical diffusion-controlled growth of nuclei. The nucleation kinetics analysis suggested that active sites on the aluminum surface played the role of critical nuclei during the initial stages of the deposition process. The addition of $[B_{mim}]HSO_4$ induced a blocking effect on the zinc electrodeposition process, leading to diminish the number of active sites for nucleus formation, decrease the nucleation and growth rate of the Zn^{2+} ions and modified the zinc crystal structure without affecting the progressive nucleation mechanism.

Key Words: Electrodeposition, Zinc, Ionic liquids, Additive, Nucleation and growth.

INTRODUCTION

Electrodeposition has received considerable interest with important application areas such as electroplating, electrometallurgy, electrocatalysis, *etc.*, as it is easier to handle and much cheaper in comparison with other modern methods[1]. Electrodeposition of zinc and its alloys have been widely investigated with the aim of obtaining films with required properties[2-4], however, the electrodeposition of zinc from aqueous solution is often complicated by problems involving hydrogen embitterment and low current efficiency[5]. In order to obtain leveled, smooth and dense deposits, the use of additives in electrolytic baths is inevitable. The quantity of additive required is always considerably small (parts per million), but their action is often specific[6]. Their presence in the electrolyte influences the nucleation and growth behaviour and therefore, promotes the formation of smooth and bright coatings. The specific activity of an additive is generally understood in terms of its adsorption onto the cathode surface during electrodeposition and this adsorption can affect the activation energy and the rate of charge transfer[7] during the electrochemical reaction and may also influence the mechanism of electrodeposition[8]. In addition, the adsorbed additives block part of the electrode surface, thereby reducing the number of active sites for the formation of nuclei and causing a decline in the nucleation rate[9,10]. The study of the initial stages is helpful to understand the nucleation process and provides important information on growth morphology at the early stages of metal deposition as it seems to be significant in determining the morphology and physicochemical properties of the electrodeposited layer[11]. Although acid sulphate bath is a classical solution for zinc electrodeposition, the nucleation mechanism in this system has not been fully studied, especially with additive in the bath.

Alvarez *et al.*[12] studied the first stages of the zinc electrodeposition on highly oriented pyrolytic graphite (HOPG) from a 0.1 M $ZnSO_4$ + 0.5 M Na_2SO_4 solution with gelatine as additive and showed that the practically instantaneous nucleation mechanism observed in the solution free of gelatine was changed to a more progressive one in the presence of gelatine in the solution. Trejo *et al.*[13,14] observed that the addition of polyethoxylated compounds had a blocking effect on the zinc electrodeposition from an acidic chloride bath and modified the nucleation process. The observed effects were dependent on the molecular weight of the polyethoxylated additive. Ballesteros *et al.*[15] claimed that polyethylene glycol 20000 (PEG20000) had induced a distinct change in the nucleation and growth mechanism of zinc electrodeposition from an acidic

chloride solution onto a steel electrode. Yu *et al*.[16] studied the temperature dependence of the electrocrystallization of zinc onto a glassy carbon (GC) electrode using cyclic voltammetry and chronoamperometry measurements and observed that increasing the temperature increased the nucleation density and modified the nucleation mechanism of Zn electrodeposition. Raeissi *et al*.[17] showed that temperature, pH and current density influenced the morphology, texture and nucleation mechanism of Zn deposits. Sonneveld *et al*.[18] reported that zinc nucleation from a zincate solution on carbon substrate can be interpreted by a model involving instantaneous nucleation in conjunction with three-dimensional hemispherical growth.

In our pervious studies, 1-butyl-3-methylimidazolium hydrogen sulphate- $[B_{mim}]HSO_4$ is found to be efficient as levelling agent for zinc[19,20] and copper[21] electrodeposition. Thus, it is interesting to investigate the effect of this ionic liquid additive on the nucleation and growth mechanism of zinc deposition. The aim of this study is to gain further insight into the early stages of zinc electrodeposition on aluminum electrode from acidic sulphate bath in the presence of $[B_{mim}]HSO_4$ as additive. Aluminum electrode has been selected as foreign substrate on account of its widely using as the cathode material for industrial hydrometallurgical electrowinning of zinc and relatively high overpotential for hydrogen evolution. Electrochemical studies were based on the analysis of cyclic voltammetric and chronoamperometric measurements. In addition, the controlled-potential bulk deposition of zinc was investigated in the absence and presence of $[B_{mim}]HSO_4$ and the resulting deposits were examined with scanning electron microscopy (SEM).

EXPERIMENTAL

The electrodeposition of zinc was studied in a 0.1 M $ZnSO_4$ + 0.5 M Na_2SO_4 solution prepared by $ZnSO_4 \cdot 7H_2O$, Na_2SO_4 and double distilled water. The solution pH was adjusted to 2.6 with 3 M H_2SO_4 addition. The ionic liquid additive 1-butyl-3-methylimidazolium hydrogen sulphate- $[B_{mim}]HSO_4$ was laboratory synthesized and the specific synthetic methods were mentioned elsewhere[19,22]. The influence of $[B_{mim}]HSO_4$ on the zinc deposition process was analyzed with adding 5 mg dm^{-3} of this additive to electrolyte, which was found to be the optimum additive concentration in the previous study[19]. All the reagents used were AR grade.

Electrochemical measurements were carried out using an electrochemical work station (GAMRY USA, PCl4/300) and based on the analysis of cyclic voltammetry and potentiostatic current-time transients. A conventional three-electrode electrochemical cell was used for these experiments. The working electrode was an aluminum disc electrode (Φ 4 mm). The counter electrode was a platinum bar electrode (Φ 1 mm × 10 mm) and the reference electrode was a saturated calomel electrode (SCE) mounted inside a Luggin capillary. Prior to each experiment, the working electrode was polished to a mirror finish using 0.5 μm high-purity alumina and then degreased with anhydrous alcohol in an ultrasonic bath for 1 min, washed with doubly distilled water and finally dried. The solution was degassed with ultrapure argon bubbling for 0.5 h prior to each experiment to avoid any reactions with dissolved oxygen.

Cyclic voltammetric experiments were carried out at a constant scan rate of 10 mV s^{-1} from the initial potential of -0.40 V to the final potential of -1.35 V. Potentiostatic current-time transients were obtained at a series of constant potentials chosen from the activation controlled region. Bulk zinc deposits were prepared on aluminum disk electrode (Φ 4 mm diameter, 99.995 %). The electrodeposited cathode was removed from the cell and washed thoroughly with distilled water and dried. A microscope (Tescan Czech, VEGA II XMH) was used to examine the surface morphology of the electrodeposits.

RESULTS AND DISCUSSION

Polarization studies: The cyclic voltammograms were recorded at 25 ºC on an aluminum electrode in the baths in absence and presence of $[B_{mim}]HSO_4$ are given in Fig. 1. The voltammograms were started from point 'A' (-0.40 V *versus* SCE), scanned in the negative direction down to a potential of -1.35 V *versus* SCE and reversed in the positive direction. The rapid increase in current observed at point 'B', is assigned to the commencement of the electroreduction of Zn^{2+} at the cathode. The point 'B' refers to the nucleation potential where zinc electrodeposition occurs on the aluminum electrode. The current increased sharply to point 'C' where the scan was reversed and then decreased and subsequently reached the point of zero current 'D', where the current became anodic corresponding to the dissolution of the deposited zinc previously formed. A current crossover is therefore observed (*ca*. -1.07 V *versus* SCE) and the appearance of such hysteresis loop is a characteristic feature of a nucleation and growth process[23]. This nucleation loop indicates that the electrodeposition of zinc on aluminum electrode during the forward scan requires an overpotential in order to initiate the nucleation and subsequent growth of the zinc deposit. Fig. 1 showed the electrodeposition of zinc from the bath with the addition of $[B_{mim}]HSO_4$ requires a larger overpotential (*ca.* 50 mV) than the additive-free one, simultaneously with the reduction of cathodic process area, denoting an inhibition of the electrocrystallization. This is generally attributed to the surface coverage of the cathode by a strongly adsorption of additive on the active sites, which blocks the interface for the electrodeposition. In this case, additional energy was required to discharge the metal ions and consequently, the deposition overpotential was increased. In the reverse scan, an oxidation peak is recorded at point 'E' (the potential of -0.95 V *versus* SCE) as a consequence of the incomplete stripping of the electrodeposits. The ratio of anodic to cathodic charge is lower than one, revealing some irreversibility of this system. This behaviour could be explained in terms of some residual zinc has alloyed with aluminum on the electrode surface. The formation of intermetallic compounds during electrodeposition is often observed on metallic electrodes[24].

Chronoamperometric analysis: Chronoamperometry experiments were carried out in order to investigate the zinc nucleation/growth process in detail. These experiments were performed at different overpotentials chosen from the activation controlled region during zinc electrodeposition on aluminum from a solution of 0.1 M $ZnSO_4$ + 0.5 M Na_2SO_4,

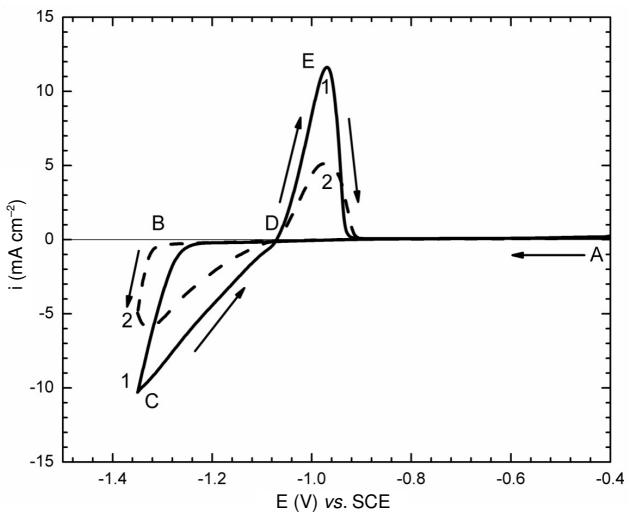

Fig. 1. Cyclic voltammograms for zinc deposition on aluminum electrode from solution 0.1 M $ZnSO_4$ + 0.5 M Na_2SO_4, pH 2.6, (1) in the absence and (2) presence of 5 mg dm^{-3} $[B_{mim}]HSO_4$

pH 2.6, in the absence and presence of 5 mg dm^{-3} $[B_{mim}]HSO_4$. The shape of the current transients is typical of diffusion-limited nucleation and growth of a metal on a foreign metal substrate (Fig. 2). The transients are characterized by an initial regime of current decay due to double-layer charging after the application of the potential pulse followed by a brief induction period, t_0[25]. At the conclusion of this induction period, the current increases due to an increase in the electroactive area as independent nuclei grow and/or the number of nuclei increases. The rising current eventually terminates in a broad maximum (i_m) as the individual diffusion zones of the growing crystallites coalesce. After i_m has been reached, the current follows the $t^{-1/2}$ decay approaching the limiting form for linear diffusion of the electroactive ions to a planar electrode, i_e, the Cottrell equation[26]:

$$I = nFSc\left(\frac{D}{\pi}\right)^{1/2} t^{-1/2} \quad (1)$$

where S represents the electrode area, D is the diffusion coefficient, n and F are the number of electrons and Faraday's constant, respectively, c is the metal ion bulk concentration and all other symbols have their usual meaning. As can be seen from the current-time transients, the time at which i_m occurs, t_m, depends on the applied overpotential, $\eta = |E - E_{eq}|$. When the applied deposition potential becomes more negative, the nucleation current increases and this shortens the time required for the diffusion zones to overlap (Fig. 2a). As a result, the observed i_m increases and t_m decreases at a more negative potential. Tables 1 and 2 list the values of i_m and t_m as a function of η that were taken from the current-time transients resulting from a typical experiment. It can also be seen from Fig. 2b that the higher overpotential value is required to initiate the nucleation and subsequent growth of the zinc deposits with the addition of $[B_{mim}]HSO_4$ in the electrolyte, denoting an inhibition of the zinc electrodeposition process. This result may be associated with the adsorption of the additive on the substrate surface, which diminishes the number of active sites for nucleus formation, decreases the nucleation and growth rate of the Zn^{2+} ions. Therefore, the higher overpotentials were needed to obtain a current maximum in the potentiostatic transients in the solution containing $[B_{mim}]HSO_4$.

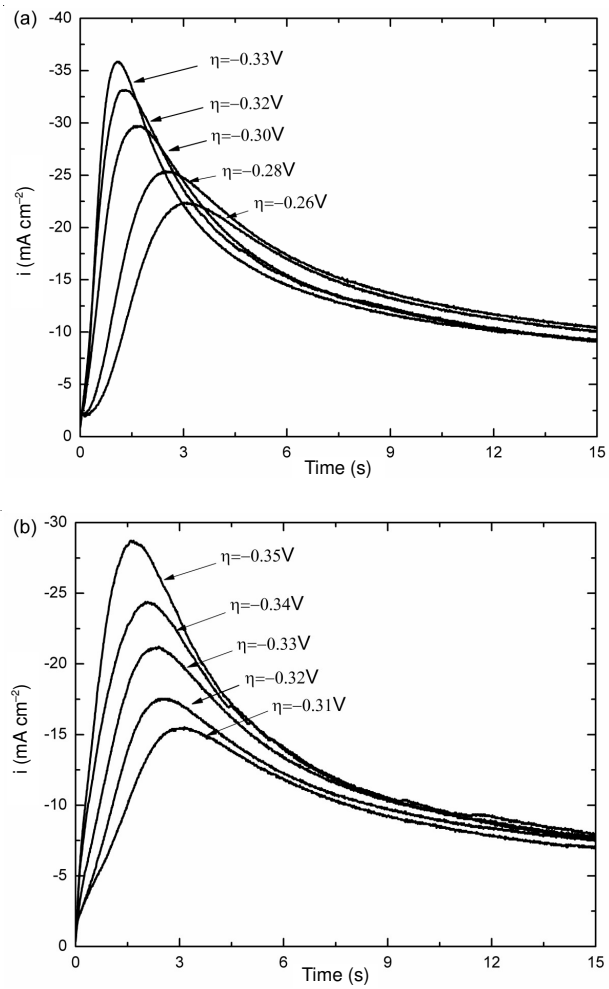

Fig. 2. Typical family of potentiosatic transients for the nucleation of zinc on aluminum at different overpotentials η, from solution 0.1 M $ZnSO_4$ + 0.5 M Na_2SO_4, pH 2.6, (a) in the absence and (b) presence of 5 mg dm^{-3} $[B_{mim}]HSO_4$

TABLE-1
CHRONOAMPEROMETRIC PARAMETERS FOR ZINC NUCLEATION ON ALUMINUM FROM THE SOLUTION WITHOUT ADDITIVE

η (V)	i_{max}/mA (cm^{-2})	t_{max} (s)	t_0 (s)	$10^{-4}AN_0$ (s^{-1} cm^{-2})	$10^{-3}N_s$ (cm^{-2})
-0.26	-22.39	3.22	0.162	0.172	3.04
-0.28	-25.41	2.48	0.148	0.295	3.99
-0.30	-29.71	1.64	0.126	0.700	6.14
-0.32	-33.14	1.28	0.100	1.153	7.88
-0.33	-35.84	1.06	0.097	1.731	9.66

TABLE-2
CHRONOAMPEROMETRIC PARAMETERS FOR ZINC NUCLEATION ON ALUMINUM FROM THE SOLUTION IN THE PRESENCE OF 5 mg dm^{-3} $[B_{mim}]HSO_4$

η (V)	i_{max} (mA cm^{-2})	t_{max} (s)	t_0 (s)	$10^{-4}AN_0$ (s^{-1} cm^{-2})	$10^{-3}N_s$ (cm^{-2})
-0.31	-15.47	3.04	0.118	0.317	5.37
-0.32	-16.70	2.68	0.120	0.413	6.13
-0.33	-21.24	2.40	0.094	0.509	6.80
-0.34	-24.40	2.07	0.090	0.690	7.92
-0.35	-28.72	1.60	0.089	1.185	10.4

To identify the nucleation mechanism, several models have been developed to describe the diffusion controlled nucleation and growth process. Two limiting cases can be observed *i.e.*, instantaneous nucleation, where all nuclei are formed immediately after the potential step and progressive nucleation, where the number of nuclei increases during the whole deposition process. An excellent method for discriminating between these two limiting nucleation/growth models was proposed by Sharifker and Hills[26]. By comparing data from the entire experimental current-time transient to the appropriate dimensionless theoretical equation derived on the basis of the models. The expressions given in eqns. 2 and 3 relate the dimensionless current to the dimensionless time for diffusion controlled three-dimensional instantaneous and progressive nucleation and growth, respectively. The resulting expressions for these quantities for both cases are given in Table-3.

$$\left(\frac{i}{i_m}\right)^2 = 1.9542\left\{1-\exp\left[-1.2564\left(\frac{t}{t_m}\right)\right]\right\}^2\left(\frac{t}{t_m}\right)^{-1} \quad (2)$$

$$\left(\frac{i}{i_m}\right)^2 = 1.2254\left\{1-\exp\left[-2.3367\left(\frac{t}{t_m}\right)^2\right]\right\}^2\left(\frac{t}{t_m}\right)^{-1} \quad (3)$$

However, in order to make an effective comparison between theory and experiment, the data must first be corrected for t_0 by redefining the time axis as $t' = t - t_0$ and the time at which i_m is observed as $t'_m = t_m - t_0$. t_0 could be obtained from the intercept of the straight lines of $i^{2/3}$ *versus* t[27]. The resulting values of t_0, are shown in Tables 1 and 2. In Fig. 3, the experimental dimensionless current-time transients from several experiments are compared to the theoretical transients that were calculated from eqs. 2 and 3. From this figure, it is apparent that the experimental data are in excellent agreement with the limiting model for progressive nucleation, indicating that the electrodeposition occurred by 3D progressive nucleation on the active sites with nuclei growing at the diffusion-limited rate. The transients obtained from the solution in the presence of $[B_{mim}]HSO_4$ are qualitatively similar to the obtained in the absence of the additive, which means that the early stages of the nucleation and growth mechanism for the zinc electrodeposition process is not changed with the addition of this additive. The major difference is that the higher overpotential value is required to initiate the nucleation and subsequent growth of the zinc deposits. This observation is in agreement with the cyclic voltammetric results.

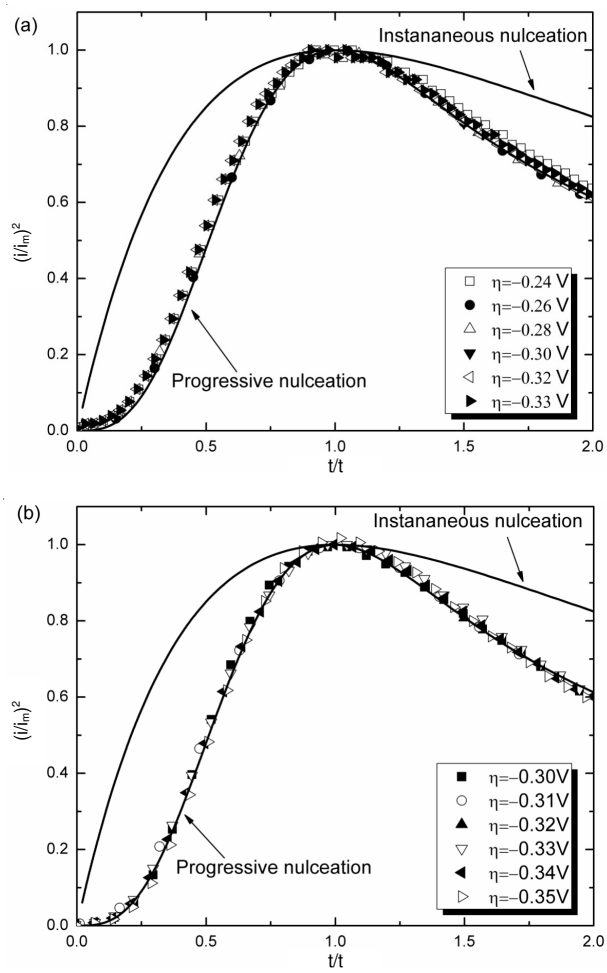

Fig. 3. Comparison of the dimensionless experimental current-time transients derived from the data in Fig. 2 with the theoretical curves for three-dimensional instantaneous and progressive nucleation of zinc on aluminum (a) in the absence and (b) presence of 5 mg dm^{-3} $[B_{mim}]HSO_4$

The transients may be used to determine several nucleation parameters: the diffusion coefficient of the electroactive species, D; the number density of active sites, N_0; nucleation rate per site, A. For the present case, the diffusion coefficients for the Zn^{2+} ions in both solution conditions, without (D_0) and with $[B_{mim}]HSO_4$ (D_B), were calculated separately by linearization of the falling part of the transients for long times according to the Cottrell equation. The corresponding values were $D_0 = 1.45 \times 10^{-5}$ cm^2 s^{-1} and $D_B = 8.57 \times 10^{-6}$ cm^2 s^{-1}. These parameters were used for the evaluation of the N_0 and

TABLE-3
EXPRESSIONS RESULTING FROM THE ANALYSIS OF THE CURRENT MAXIMA FOR 3D INSTANTANEOUS AND PROGRESSIVE NUCLEATION

Instantaneous nucleation		Progressive nucleation	
$t_m = \frac{1.2564}{N_0\pi kD}$	(a)	$t_m = \left(\frac{4.6733}{AN_\infty\pi k'D}\right)^{1/2}$	(e)
$i_m = 0.6382zFDc(KN_0)^{1/2}$	(b)	$i_m = 0.4615zFD^{3/4}c(k'AN_\infty)^{1/4}$	(f)
$i_m^2 t_m = 0.1629(zFc)^2 D$	(c)	$i_m^2 t_m = 0.2598(zFc)^2 D$	(g)
$\left(\frac{i}{i_m}\right)^2 = 1.9542\left\{1-\exp\left[-1.2564\left(\frac{t}{t_m}\right)\right]\right\}^2\left(\frac{t}{t_m}\right)^{-1}$	(d)	$\left(\frac{i}{i_m}\right)^2 = 1.2254\left\{1-\exp\left[-2.3367\left(\frac{t}{t_m}\right)^2\right]\right\}^2\left(\frac{t}{t_m}\right)^{-1}$	(h)

A values. However, for the limiting case of progressive nucleation, the ratio $A/N_0 \rightarrow 0$. In this case, A and N_0 cannot be determined separately and the nucleation kinetics must be analyzed in terms of the steady-state nucleation rate, AN_0, which can be calculated according to the following equation:

$$AN_0 = \frac{4.6733}{\pi k' D t_m'^2} \quad (4)$$

$$k' = \frac{4}{3}\left[\frac{(8\pi cM)}{\rho}\right]^{1/2} \quad (5)$$

where D is the diffusion coefficient of the electroactive species, M and ρ are the molecular weight and density of the metal deposit, respectively, c is the metal ion bulk concentration. The results of this calculation are collected in Tables 1 and 2 along with values of the saturation nuclear number density, N_s, which is calculated from AN_0 according to the following equation:

$$N_s = \left(\frac{AN_0}{2k'D}\right)^{1/2} \quad (6)$$

N_s is the saturation nuclear number density observed at long times after the development of new nuclei has been arrested by the formation of nucleation exclusion zones around the growing nuclei. The variation of N_s as a function of the deposition potential is shown in Fig. 4. ln N_s varies exponentially linearly with the deposition potential and decreases in the presence of additive, suggesting that a change in the critical radius of the nuclei[28]. These results suggest that the addition of additive seems to hinder the zinc nucleation. Probably some of the imidazolium molecules had adsorbed on the surface of the substrate and reduced the number of active sites for nucleation or the adsorbed imidazolium molecules give rise to a decrease in the potential available to drive the electron transfer. The process is consistent with the progressive nucleation predicted previously. On the other hand, in the presence of additive, N_s increases as the potential is changed to more negative values (Table-2). This behaviour may be attributed to the contribution of the additive on the existence of a distribution of site energies on the surface. As the cathodic overpotential increases, a larger fraction of sites become active[29].

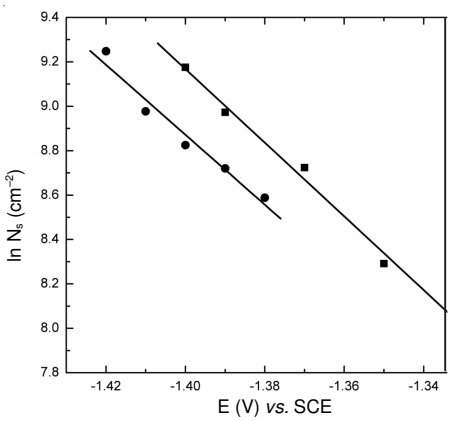

Fig. 4. Variation of the saturation nuclear number density of formed nuclei (N_s) with the deposition potential from the baths (■) in the absence and (●) presence of 5 mg dm^{-3} $[B_{mim}]HSO_4$

As shown in Fig. 5, the dependence of AN_0 with the deposition potential could be interpreted on the basis of the atomistic theory of electrolytic nucleation[12,25]. According to the atomistic theory of nucleation, the slope of a plot of log (AN_0) *versus* η gives information about the critical number of atoms required for the formation of a stable nucleus, n_k.

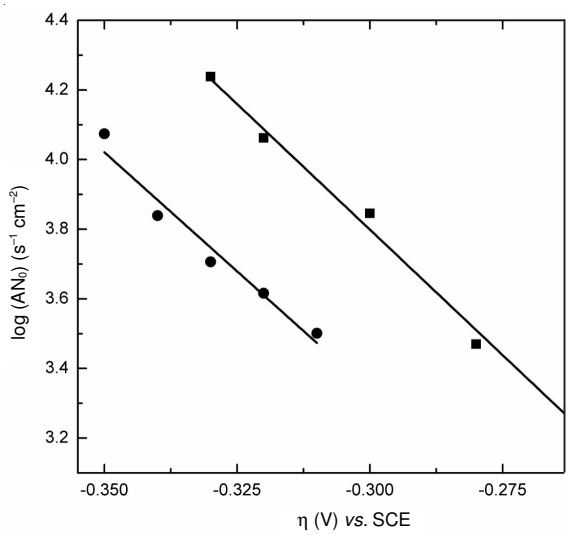

Fig. 5. Overpotential dependence of the steady-state nucleation rate, AN_0, (■) in the absence and (●) presence of 5 mg dm^{-3} $[B_{mim}]HSO_4$ in the baths

$$n_k\left(\frac{2.303RT}{zF}\right)\left[\frac{d\log(AN_0)}{d\eta}\right] \quad (7)$$

From the slope of the straight lines in Fig. 5 and using eqn. 7, $n_k \approx 0.40$ for both cases *i.e.*, in absence and presence of $[B_{mim}]HSO_4$ in the bath. The values of n_k ranging from 0 to 1 were observed for the electrodeposition of copper[30], cadmium[31], lead[32] and silver[33] on glassy carbon in aqueous solutions, which indicated that each active site on the electrode surface possibly acts as effectively as a critical nucleus[34] during the electrodeposition of zinc. Therefore, it may be inferred that the addition of $[B_{mim}]HSO_4$ did not drastically change the size of the critical nucleus. The action of $[B_{mim}]HSO_4$ could be ascribed to a higher blocking effect of the additive and/or to a decrease of the rate of the ions transferred across the electric double layer[28].

Morphological studies: The surface morphology of zinc deposits produced on an aluminum electrode from the bath in absence and presence of $[B_{mim}]HSO_4$ for a fixed deposition potential and approximately the same amount of charge are shown in Fig. 6. In the absence of additive, the deposit obtained is in the form of hemispherical hexagonal plates with similar sizes (Fig. 6a and c) as is typical for the pure zinc electrodeposits[35,36]. In the presence of additive, the zinc crystal structure obtained is found to be modified and the deposits are formed by flakes grouped in clusters with slightly increase in crystallites size (Fig. 6b and d). This result is expected on account for the blocking effect of the additive through cathodic adsorption on the electrode surface that causes a reduction in both the number of the active sites and nucleation rate of nuclei, resulting in an increase in grain size. Such increases in the

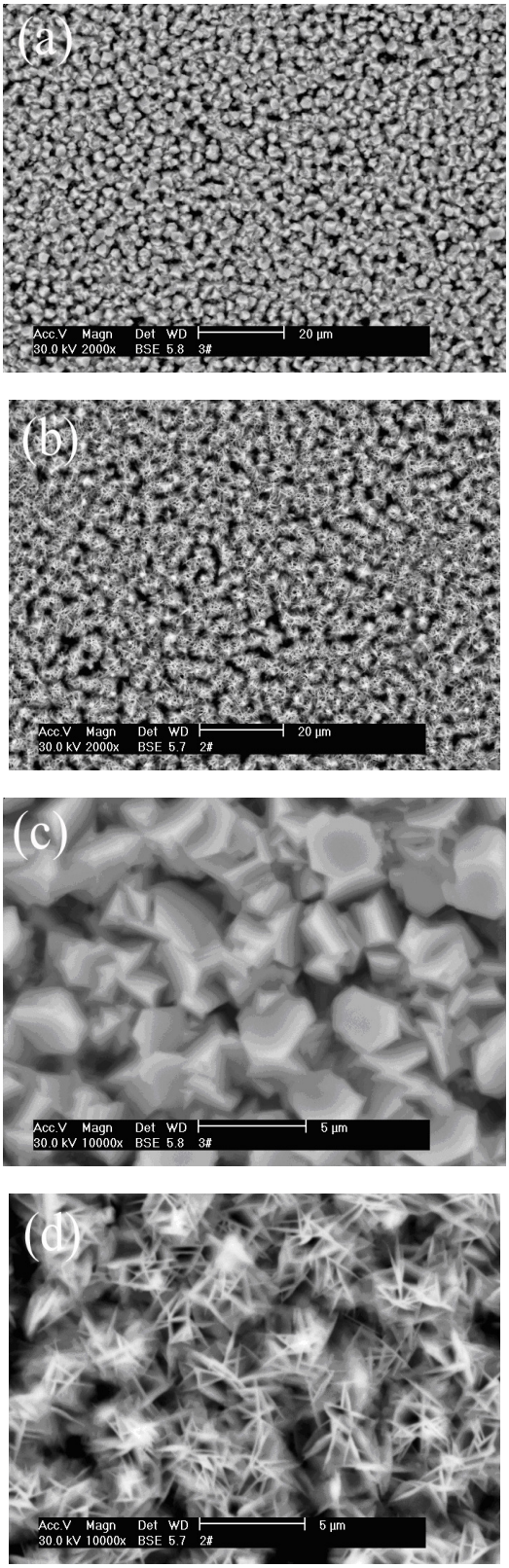

Fig. 6. SEM micrographs of zinc electrodeposits produced on aluminum from solution 0.1 M $ZnSO_4$ + 0.5 M Na_2SO_4, pH 2.6 (a, c) in the absence and (b, d) presence of 5 mg dm^{-3} $[B_{mim}]HSO_4$ at 25 ºC. The deposition potential was -1.35 V and Q = 1.00 ± 0.01C

crystallites size of the nuclei with the addition of additive have also been observed by other workers[13] for zinc electrodeposition in the presence of organic polyethoxylated additives from an acidic chloride solution and are generally attributed to the surface coverage of the cathode by a strongly adsorbed additive, which decreases the zinc nucleation rate.

Conclusion

The nucleation and growth mechanism of the zinc electrodeposition on aluminum electrode from acidic sulfate bath were investigated in absence and presence of $[B_{mim}]HSO_4$ as additive. Cyclic voltammetry studies showed the electrodeposition of zinc for both cases were associated with a nucleation and growth process. From the analysis of the corresponding dimensionless chronoamperometric current-time transients, the initial stages of the zinc electrodeposition process could be explained on the basis of a three-dimensional progressive nucleation with diffusion controlled growth of the nuclei. The addition of $[B_{mim}]HSO_4$ led to diminish the number of active sites for nucleus formation, decrease the nucleation and growth rate of the Zn^{2+} ions and produce cathodic deposits with slightly increase in grain size, however, the progressive nucleation mechanism involved for the deposition process was practically unchanged. The result was produced by the blocking effect of $[B_{mim}]HSO_4$ on the zinc electrodeposition process through its cathodic adsorption on the electrode surface.

ACKNOWLEDGEMENTS

The authors gratefully acknowledged the financial support of the Natural Science Foundation of Yunnan Province (Project No. 2011FA009) and the Application Foundation Research of Yunnan Province (Project No. 2011FZ020).

REFERENCES

1. A. Sahari, A. Azizi, N. Fenineche, G. Schmerber and A. Dinia, *Mater. Chem. Phys*., **108**, 345 (2008).
2. R. Renuka, S. Ramamurthy and K. Muralidharan, *J. Power Sources*, **20**, 197 (1998).
3. J.J. Kelly, C. Tian and A.C. West, *J. Electrochem. Soc*., **146**, 2540 (1999).
4. F. Ganne, C. Cachet, G. Maurin, R. Wiart, E. Chauveau and J. Petitjean, *J. Appl. Electrochem*., **30**, 665 (2000).
5. Y.F. Lin and I.W. Sun, *Electrochim. Acta*, **44**, 2771 (1999).
6. L. Oniciu and L. Muresan, *J. Appl. Electrochem*., **21**, 565 (1991).
7. D.J. MacKinnon and J.M. Brannen, *J. Appl. Electrochem*., **12**, 21 (1982).
8. E. Michailova, M. Peykova, D. Stoychev and A. Milchev, *J. Electroanal. Chem*., **366**, 195 (1994).
9. L. Simanavicus, A. Stakenas and A. Sarkis, *Electrochim. Acta*, **42**, 1581 (1997).
10. E. Michailova, I. Vitanova, D. Stoychev and A. Milchev, *Electrochim. Acta*, **38**, 2455 (1993).
11. E. Budevski, G. Staikov and W.J. Lorenz, Electrochemical Phase Formation and Growth, Wiley-VCH, New York (1996).
12. A.E. Alvarez and D.R. Salinas, *J. Electroanal. Chem*., **566**, 393 (2004).
13. G. Trejo, H. Ruiz, R.O. Borges and Y. Meas, *J. Appl. Electrochem*., **31**, 685 (2001).
14. G. Trejo, R. Ortega and Y. Meas, *Plat. Surf. Finish*, **89**, 84 (2002).
15. J.C. Ballesteros, P. D´iaz-Arista, Y. Meas, R. Ortega and G. Trejo, *Electrochim. Acta*, **52**, 3686 (2007).
16. J. Yu, L. Wang, L. Su, X. Ai and H. Yang, *J. Electrochem. Soc*., **150**, C19 (2003).
17. K. Raeissi, A. Saatchi and M.A. Golozar, *J. Appl. Electrochem*., **33**, 635 (2003).
18. P.J. Sonneveld, W. Visscher and E. Barendrecht, *Electrochim. Acta*, **37**, 1199 (1992).
19. Q.B. Zhang and Y.X. Hua, *J. Appl. Electrochem*., **39**, 261 (2009).
20. Q.B. Zhang and Y.X. Hua, *J. Appl. Electrochem*., **39**, 1185 (2009).
21. Q.B. Zhang, Y.X. Hua, Y.T. Wang, H.J. Lu and X.Y. Zhang, *Hydrometallurgy*, **98**, 291 (2009).

22. J.A. Whitehead, G.A. Lawrance and A. McCluskey, *Aust. J. Chem*., **57**, 151 (2004).
23. S. Fletcher, C.S. Halliday, D. Gates, M. Westcott, T. Lwin and G. Nelson, *J. Electroanal. Chem*., **159**, 267 (1983).
24. B. Lazar, A. Nishri and S. Ben-Yaakov, *J. Electroanal. Chem*., **125**, 295 (1981).
25. W.R. Pitner and C.L. Hussey, *J. Electrochem. Soc*., **144**, 3095 (1997).
26. B.R. Scharifker and G. Hills, *Electrochim. Acta*, **28**, 879 (1983).
27. P.M. Rigano, C. Mayer and T. Chierchie, *J. Electroanal. Chem*., **248**, 219 (1988).
28. G. Trejo, A.F. Gil and I. Gonzalez, *J. Electrochem. Soc*., **142**, 3404 (1995).
29. E. Michailova, I. Vitanova, D. Stoychev and A. Milchev, *Electrochim. Acta*, **38**, 2455 (1993).
30. G. Gunawardena, G. Hills and I. Montenegro, *J. Electroanal. Chem*., **184**, 357 (1985).
31. G. Gunawardena, G. Hills and I. Montenegro, *J. Electroanal. Chem*., **184**, 371 (1985).
32. J. Mostany, J. Parra and B.R. Scharifker, *J. Appl. Electrochem*., **16**, 333 (1986).
33. G. Gunawardena, G. Hills and I. Montenegro, *J. Electroanal. Chem*., **138**, 241 (1982).
34. A. Milchev, S. Stoyanov and R. Kaischev, *Thin Solid Films*, **22**, 255 (1974).
35. G. Barceló, M. Sarret, C. Müller and J. Pregonas, *Electrochim. Acta*, **43**, 13 (1998).
36. H. Yan, J. Downes, P.J. Boden and S.J. Harris, *J. Electrochem. Soc*., **143**, 1577 (1996).